Structural Characterization of Verdoheme Analogs. Iron Complexes of Octaethyloxoporphyrin

Alan L. Balch,*,† Lechosław Latos-Grażyński,‡ Bruce C. Noll,† Marilyn M. Olmstead,† Ludmiła Szterenberg,‡ and Nasser Safari†

Contribution from the Department of Chemistry, University of California, Davis, California 95616, and Institute of Chemistry, University of Wrocław, Wrocław, 58383 Poland. *Received July 23, 1992*

Abstract: The verdohemes are shown to contain the planar, tetradentate oxoporphyrin structure. Structural studies of paramagnetic {(OEOP)$Fe^{III}Cl_2$}, where OEOP is the monoanion of octaethyloxoporphyrin, by ^1H NMR spectroscopy and X-ray crystallography reveal that the iron is six-coordinate and high-spin ($S = {}^5/_2$). The iron resides in the plane of the oxoporphyrin and is coordinated by two equivalent axial chloride ligands. Paramagnetic {(OEOP)$Fe^{II}Cl$} contains a five-coordinate iron which is also high-spin ($S = 2$). The iron is 0.69 Å out of the porphyrin plane and bound to a single axial chloride. The average Fe–N distance increases from 1.964 Å in the iron(III) complex to 2.094 Å in the iron(II) complex. {(OEOP)$Fe^{III}Cl_2$} was obtained by treatment of (OEP)$Fe(py)_2$ (OEP is the dianion of octaethylporphyrin) with dioxygen in the presence of ascorbic acid to form the verdohemochrome [(OEOP)$Fe^{II}(py)_2$]Cl, which was subsequently reacted with hydrogen chloride in air. Reduction of {(OEOP)$Fe^{III}Cl_2$} with sodium dithionite yields air-sensitive {(OEOP)$Fe^{II}Cl$}. When {(OEOP)$Fe^{II}Cl$} is dissolved in pyridine, [(OEOP)$Fe^{II}(py)_2$]Cl is reformed.

Introduction

The ability of metalloporphyrins and the heme enzymes, particularly cytochrome P-450, to catalyze a remarkable range of oxidations that utilize molecules of oxygen as the oxidant has received an extraordinary degree of attention for well over a decade.[1,2] As a result, considerable advances have been made in understanding what species are involved in these important processes, and it is clear that in the appropriate protein environment the heme/dioxygen combination can produce a potent oxidant.

It is also remarkable that nature is able to utilize this same heme/dioxygen combination to destroy unwanted heme.[3-5] Catabolism of heme produces bilirubin, the cause of neonatal jaundice, as shown in Scheme I. Two enzymes, heme oxygenase and bilirubin reductase, are involved. The first of these, heme oxygenase, utilizes dioxygen to carry out a regiospecific opening of the tetrapyrolic macrocycle at the α-methine position. The α-methine carbon is converted to carbon monoxide, and iron is released to give the product, biliverdin.

Oxidation of heme in pyridine by dioxygen in the presence of a reducing agent (hydrazine or ascorbic acid) has been used as a model for the heme oxygenase reaction.[6-19] This process, which is termed coupled oxidation, is generally believed to occur through the sequence of intermediates shown in Scheme II. The heme is initially hydroxylated at a meso carbon. Subsequently a green complex, (a verdoheme) is formed. On hydrolysis, this green complex can be transformed to biliverdin. In this nonenzymatic process, the regiospecificity of the enzymatic ring opening is lost and any one of the four meso carbons may be lost as carbon monoxide.

This article is concerned with structural studies on the green pigments, the verdohemes, that coupled oxidation produces. The verdoheme known as verdohemochrome is isolated in generally less than 40% yield from the coupled oxidation process. This compound has been formulated as an iron(II) complex with two axial pyridine ligands. Verdohemochrome is converted into verdohemin by treatment with hydrogen chloride with air. This process was believed to remove the pyridine ligands and oxidize the iron(II) to iron(III). Two structures A and B have been proposed for the tetrapyrrolic macrocycle in verdohemochrome.[7,12,13] Despite chemical evidence and NMR spectral data on the verdohemochrome that are consistent with the more symmetrical structure[10,12,13] A, structure B still appears in the chemical literature.[19] Generally, studies of the verdohemes have given limited attention to rigorous identification of the coordination geometry of the iron and the details of its electronic structure. With verdohemin, for example, structures with four-,[7] five-,[18] and six-coordinate[10] iron have been suggested without spectroscopic or crystallographic verification.

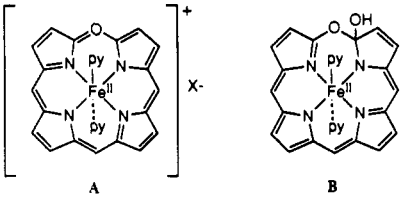

Here we report on the isolation and characterization of two verdoheme derivatives in which thorough identification of the spin, oxidation, and ligation states of iron have been made. In order to avoid the regiochemical problems encountered in the oxidation of heme itself, we have concentrated on the symmetrical analog octaethylporphyrin. The complexes we have obtained all contain the oxoporphyrin structure C with a, b, c, and d = ethyl and m, m′ = H.

Here and throughout this paper, the abbreviations used are as follow: OEP, dianion of octaethylporphyrin; OEOP, monoanion of octaethyloxoporphyrin, the tetrapyrrole ligand in structure C;

† University of California.
‡ University of Wrocław.

(1) *Cytochrome P-450*; Ortiz de Montellano, P. R., Ed.; Plenum Press: New York, 1986.
(2) Mansuy, D. *Pure Appl. Chem.* **1987**, *59*, 759.
(3) Bissell, D. M. In *Liver: Normal Function and Disease. Vol. 4, Bile Pigments and Jaundice*; Ostrow, J. D., Ed.; Marcel Decker, Inc.: New York, 1986; p 133.
(4) Schmid, R.; McDonagh, A. F. In *The Porphyrins*; Dolphin, D., Ed.; Academic Press: New York, 1979; Vol. 6, p 258.
(5) O'Cara, P. In *Porphyrins and Metalloporphyrins*; Smith, K. M., Ed.; Elsevier: New York, 1975; p 122.
(6) Warburg, O.; Negelein, E. *Chem. Ber.* **1930**, *63*, 1816.
(7) Foulkes, E. C.; Lemberg, R.; Pardonn, P. *Proc. Roy. Soc. (London)* **1951**, *B138*, 386.
(8) Lemberg, R. *Rev. Pure Appl. Chem.* **1956**, *6*, 1.
(9) Levin, E. Y. *Biochemistry* **1966**, *5*, 2845.
(10) Jackson, A. H.; Kenner, G. W.; Smith, K. M. *J. Chem. Soc.* **1968**, 302.
(11) Bonnett, R.; Dimsdale, M. J. *J. Chem. Soc., Perkin Trans. I* **1972**, *79*, 1393.
(12) Saito, S.; Itano, H. A. *Proc. Natl. Acad. Sci. U.S.A.* **1982**, *79*, 1393.
(13) Lagarias, J. C. *Biochem. Biophys. Acta* **1982**, *717*, 12.
(14) Itano, H. A.; Hirota, T. *Tetrahedron Lett.* **1983**, *24*, 995.
(15) Sano, S.; Sano, T.; Morishima, I.; Shiro, Y.; Maeda, Y. *Proc. Natl. Acad. Sci. U.S.A.* **1986**, 531.
(16) Saito, S.; Itano, H. A. *J. Chem. Soc., Perkin Trans. I* **1986**, 1.
(17) Masuoka, N.; Itano, H. A. *Biochemistry* **1987**, *26*, 3672.
(18) Saito, S.; Sumita, S.; Iwai, K.; Sano, H. *Bull. Chem. Soc. Jpn.* **1988**, *61*, 3539.
(19) Modi, S.; Behere, D. V.; Shedbalkar, V. P. *J. Chem. Res.* **1988**, 244.

0002-7863/93/1515-1422$04.00/0 © 1993 American Chemical Society

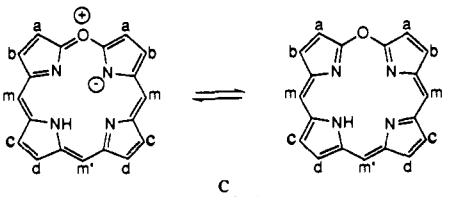

C
oxoporphyrin
OEOPH, a, b, c, d = ethyl; m, m' = hydrogen

TPP, dianion of tetraphenylporphyrin; and py, pyridine.

Results

Synthetic Studies. Verdohemochrome, $[(OEOP)Fe^{II}(py)_2]Cl$ (**2**), was prepared from $(OEP)Fe^{II}(py)_2$ (**1**) by a slight modification of the previously reported routes.[13] In our hands a 50% yield of **2** has been obtained; others have reported a 40% yield of verdohemochrome.[12] The UV/vis absorption spectrum of this complex is shown in trace A of Figure 1. This spectrum is virtually identical to those reported earlier for verdohemochromes.[9,11-13] The complex is diamagnetic and produces a ^1H NMR spectrum (see Experimental Section) that agrees with the earlier report.[12] This iron(II) complex is stable in air in solution so long as an excess of pyridine is present. In our hands the coupled oxidation process also produces a paramagnetic iron complex which accounts for another 40% of the sample. Characterization of this second material, which has not been described previously, will appear in a later publication.

Treatment of $[(OEOP)Fe^{II}(py)_2]Cl$ with hydrogen chloride in air yields $\{(OEOP)Fe^{III}Cl_2\}$ (**3**, X = Cl). The corresponding reaction with hydrogen bromide in air yields $\{(OEOP)Fe^{III}Br_2\}$ (**3**, X = Br). Reduction of $\{(OEOP)Fe^{III}X_2\}$ (X = Cl or Br) with sodium dithionite in dichloromethane results in the formation of air-sensitive $\{(OEOP)Fe^{II}X\}$ (**4**). When $\{(OEOP)Fe^{II}Cl\}$ (**4**) is dissolved in pyridine or when pyridine is added to dichloromethane solutions of this complex, $[(OEOP)Fe^{II}(py)_2]Cl$ is reformed. This reaction has been monitored by changes in the UV/vis absorption spectra and ^1H NMR spectra. These transformations are summarized in Scheme III.

Characterization of $\{(OEOP)Fe^{III}X_2\}$ (X = Cl or Br). These complexes are obtained as deep green crystals with good solubility in chloroform and dichloromethane. The electronic absorption spectrum of $\{(OEOP)Fe^{III}Cl_2\}$ is shown in trace B of Figure 1. This spectrum shows reasonable agreement with those obtained previously for samples of verdohemin from natural and synthetic porphyrins.

$\{(OEOP)Fe^{III}Cl_2\}$ is paramagnetic. Its magnetic moment, as measured by the Evans technique,[20] is 5.5(1) μ_B in chloroform solution at 23 °C.

The ^1H NMR spectrum of $\{(OEOP)Fe^{III}Cl_2\}$ at −60 °C in chloroform-*d*, shown in Figure 2, is consistent with the paramagnetic nature of the complex. At this temperature all of the resonances are well spread out and readily assigned on the basis of their intensities, line widths, and chemical shifts. Two meso resonances with an intensity ratio of 1:2 are seen at 71 and 58 ppm. Four equally intense methylene resonances are found between 90 and 45 ppm. Two methyl resonances with intensity corresponding to 24 protons are observed between 15 and 10 ppm at −60 °C. These split somewhat at higher temperatures, where the line width decreases. Figure 3 shows the spectrum at 23 °C, where this splitting is apparent in the upfield region. The line widths increase in the order methyl, methylene, meso. This is consistent with a dominant dipolar contribution to the line width (which is proportional to r^{-6})[21] since the order of distances from the iron increases from meso proton to methylene proton to methyl proton. These spectra are consistent with the structure shown in Scheme II, in which the iron is six-coordinate and both protons of each of the four methylene groups are equivalent. The temperature dependence of the ^1H NMR spectrum shows linear behavior of the chemical shifts when these are plotted versus T^{-1}. This is shown in inset B of Figure 2. However, the chemical shifts

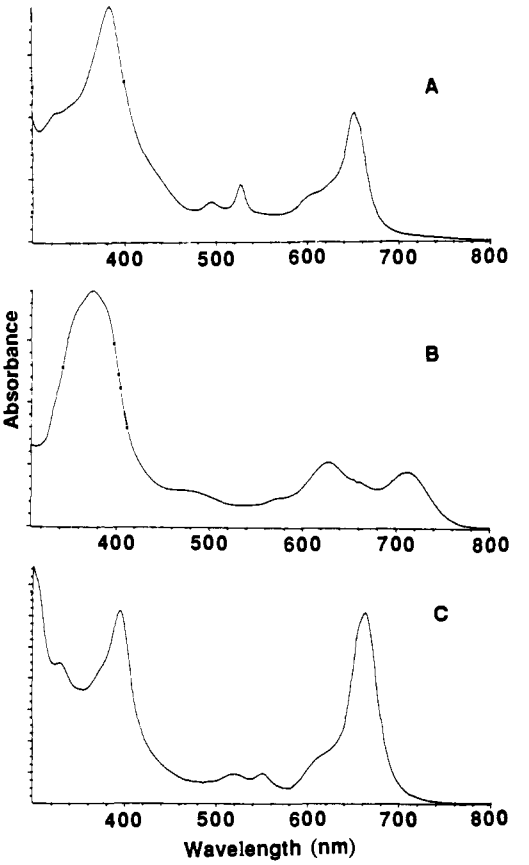

Figure 1. UV/vis absorption spectra of A, $[(OEOP)Fe^{II}(py)_2]Cl$ in dichloromethane with 1% pyridine added; B, $\{(OEOP)Fe^{III}Cl_2\}$ in dichloromethane; and C, $\{(OEOP)Fe^{II}Cl\}$ in dichloromethane.

Scheme I

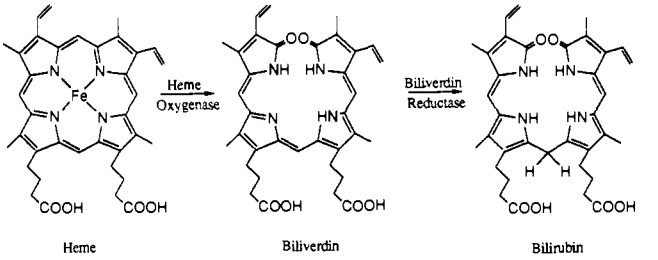

Scheme II. Coupled Oxidation[a]

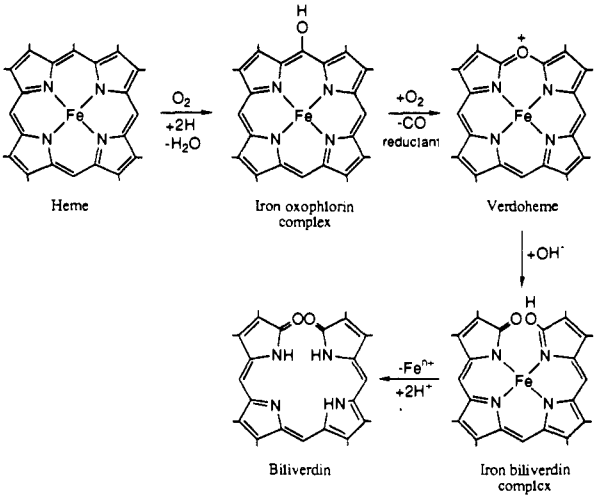

[a] Iron ligation and oxidation states unspecified.

(20) Evans, D. F. *J. Chem. Soc.* **1959**, 2003.
(21) Swift, T. J. In *NMR of Paramagnetic Molecules*; La Mar, G. N., Horrocks, W. D., Jr., Holm, R. H., Eds.; Academic Press: New York, 1973; p 53.

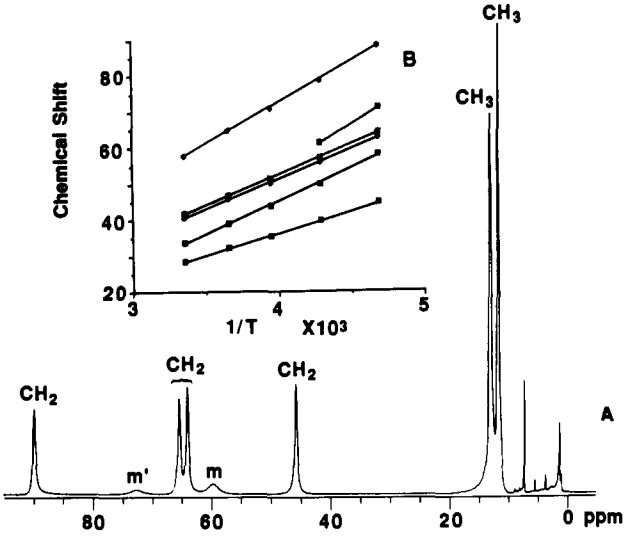

Figure 2. A, 300-MHz ^{1}H NMR spectrum of {(OEOP)Fe^{III}Cl$_2$} in chloroform-*d* at −60 °C. Resonances are identified as m, m′ = meso protons, CH_2 = methylene protons, and CH_3 = methyl protons. B, a plot of chemical shifts versus T^{-1} for the methylene and meso proton resonances. The low-field meso resonance merges with the methylene resonances on warming, and consequently its position is shown at only two temperatures.

Scheme III

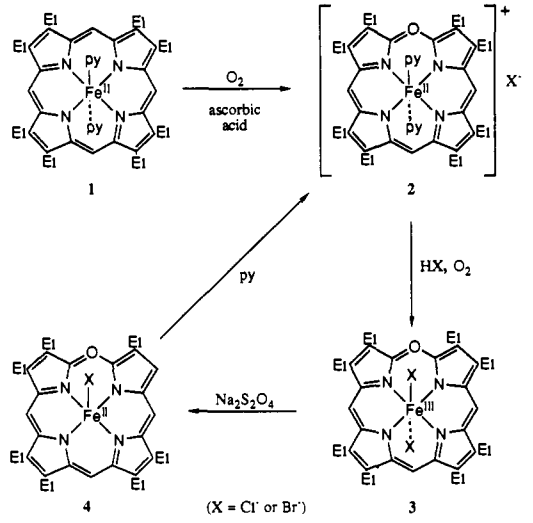

do not extrapolate at infinite temperature to the positions anticipated for a diamagnetic material.

Two-dimensional magnitude COSY (MCOSY) experiments are effective in determining the sets of resonances that belong to a single ethyl group in paramagnetic complexes.[22] Cross peaks are expected between resonances of each unique ethyl group for which couplings of ca. 14 Hz between geminal protons and ca. 7 Hz between vicinal protons are anticipated as a result of studies on diamagnetic complexes.

Figure 3 shows an MCOSY map that was obtained for {(OEOP)Fe^{III}Cl$_2$} in chloroform-*d* at 23 °C. The top shows the normal spectrum, while the lower part is the MCOSY map. Cross peaks that connect the spin-coupled protons of the methylene and methyl groups are readily apparent. As expected, the cross peaks for the two narrower methylene resonances are stronger than the cross peaks that correspond to the broader methylene resonances.

The structure of {(OEOP)Fe^{III}Br$_2$}·$C_4H_{10}O$, as determined by X-ray crystallography, is shown in Figure 4. Relevant bond distances and angles are given in Table I. The complex has crystallographically imposed C_{2h} symmetry. Consequently, the

(22) Keating, K. A.; de Ropp, J. S.; La Mar, G. N.; Balch, A. L.; Shiau, F.-Y.; Smith, K. M. *Inorg. Chem.* **1991**, *30*, 3258.

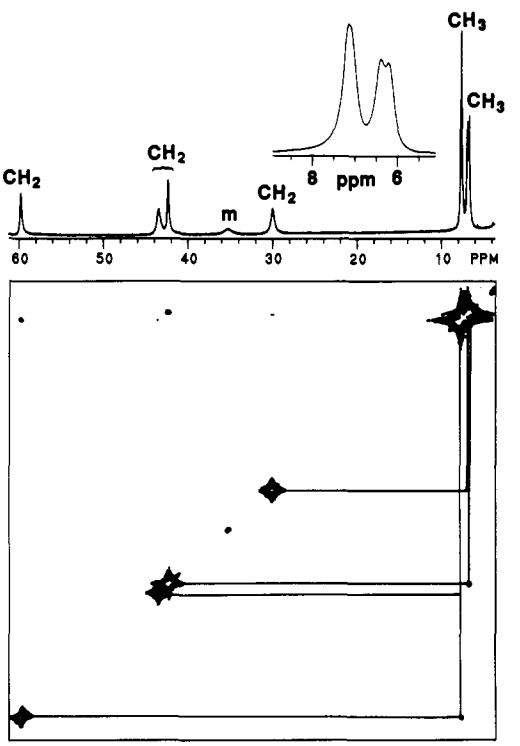

Figure 3. Top: 300-MHz ^{1}H NMR spectrum of {(OEOP)Fe^{III}Cl$_2$} in chloroform-*d* at 23 °C. The inset shows an expansion of the methyl peaks between 6 and 8 ppm. Bottom: 300-MHz ^{1}H MCOSY plot for {(OEOP)Fe^{III}Cl$_2$}. Cross peaks between the resonances of methylene and methyl protons are connected below the diagonal. Resonance labels follow those in Figure 2.

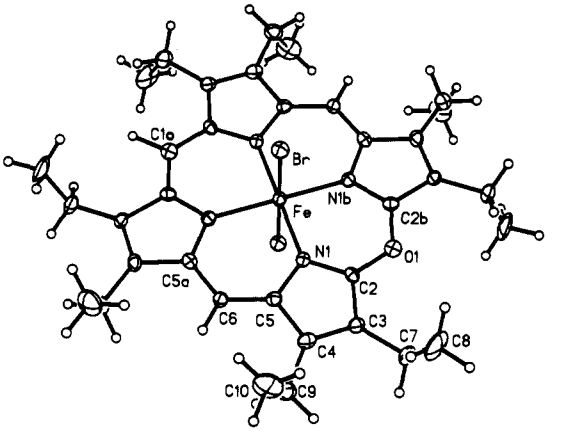

Figure 4. Perspective view of the structure of {(OEOP)Fe^{III}Br$_2$} with 50% thermal contours for all atoms.

Table I. Selected Interatomic Distances and Angles for {(OEOP)Fe^{III}Br$_2$}·OC_4H_{10}

Bond Distances (Å)			
Fe–Br	2.430(1)	Fe–N(1)	1.964(5)
N(1)–C(2)	1.352(7)	N(1)–C(5)	1.387(8)
O(1)–C(2)	1.368(7)	C(1)–C(2)	1.368(7)
C(2)–C(3)	1.446(9)	C(3)–C(4)	1.358(8)
C(4)–C(5)	1.446(8)	C(5)–C(6)	1.379(7)
Bond Angles (deg)			
Br–Fe–N(1)	90.1(1)	N(1)–Fe–N(1B)	89.3 (3)
Fe–N(1)–C(2)	128.3(4)	Fe–N(1)–C(5)	127.7(3)
C(2)–N(1)–C(5)	104.0(5)	C(2)–O(1)–C(2A)	125.1(7)
C(2)–C(1)–C(2A)	125.1(7)	N(1)–C(2)–O(1)	124.5(5)
N(1)–C(2)–C(1)	124.5(5)	N(1)–C(2)–C(3)	112.8(5)
O(1)–C(2)–C(3)	122.7(5)	C(1)–C(2)–C(3)	122.7(5)
C(2)–C(3)–C(4)	105.6(5)	C(3)–C(4)–C(5)	106.5(5)
N(1)–C(5)–C(4)	111.1(5)	N(1)–C(5)–C(6)	123.7(5)
C(4)–C(5)–C(6)	125.2(6)	C(5)–C(6)–C(5A)	126.4(8)

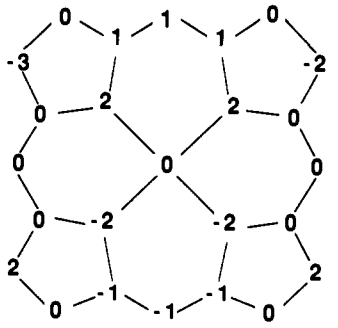

Figure 5. Diagram of the oxoporphyrin core for {(OEOP)Fe^{III}Br$_2$}. Each atom symbol has been replaced by a number that represents the perpendicular displacement (in units of 0.01 Å) from the mean plane of the oxoporphyrin core.

asymmetric unit consists of one fourth of the complex. The mirror plane contains Fe, Br, and C(6). The C_2 axis passes through Fe, C(1), and O(1). The structure suffers from disorder that involves the location of the oxygen atom and one of the meso methine groups. Thus C(1) and O(1) share a common position. The other methine position is not involved in the disorder. The hydrogen atoms of the ethyl groups and the hydrogen atom connected to the methine carbon C(6) were located on a difference map. That map also showed a peak of one-half the size of a hydrogen adjacent to O/C(1). This was treated as the methine hydrogen of this disordered part of the structure. Figure 4 shows the entire molecule with the disorder removed. The iron is six-coordinate. The Fe–N bond distance, 1.964(5) Å, is shorter than the Fe–N distance of 2.045–2.065 expected for high-spin, six-coordinate iron(III) porphyrin complexes.[23,24] The Fe–Br distance, 2.430(1) Å, is longer than the Fe–Br distance (2.348(2) Å) in high-spin, five-coordinate {(TPP)Fe^{III}Br}.[25] The oxoporphyrin skeleton is essentially planar. Figure 5 shows a diagram which gives the out-of-plane distances for the atoms of this core.

Characterization of {(OEOP)Fe^{II}X} (X = Cl or Br). These complexes are obtained as deep green crystals which have good solubility in chloroform and dichloromethane. The electronic absorption spectrum obtained from a chloroform solution of {(OEOP)Fe^{II}Cl} is shown in trace C of Figure 1. This absorption spectrum is clearly different from that of {(OEOP)Fe^{III}Cl$_2$} but is very similar to that of [(OEOP)Fe^{II}(py)$_2$]Cl.

In dichloromethane solution, {(OEOP)Fe^{II}Cl} has a magnetic susceptibility of 4.9(1) μ_B at 23 °C. This is consistent with a high-spin (S = 2) electronic configuration for the complex.

Trace A of Figure 6 shows the ^{1}H NMR spectrum of (OEOP)Fe^{II}Cl in dichloromethane-d_2 at 30 °C. The methylene and methine protons show strong paramagnetic shifts that place them in the downfield region. The two methine resonances are readily assigned on the basis of their intensity. Their greater line width is consistent with the fact that they are the protons in the complex which are closest to the iron and hence that they are the most affected by dipolar relaxation. There are eight clearly resolved, equally intense methylene resonances which span the range 31 to 7 ppm. Since the iron is five-coordinate (vide infra), each of the two methylene protons of the four unique ethyl groups is chemically distinct and hence there are eight methylene resonances. Three methyl resonances, one with double the intensity of the other two, are seen in the 0–5 ppm region. The effects of temperature on the methylene resonances are shown in inset B. The plots follow the Curie law. At infinite temperature, these plots extrapolate to the range from 5 to −3 ppm, which is reasonably close to what is expected for the methylene region for a diamagnetic porphyrin.

For each ethyl group, a characteristic pattern with three cross peaks is seen. The 300-MHz MCOSY plot for {(OEOP)Fe^{II}Cl} at 30 °C in dichloromethane-d_2 is shown in Figure 7. These results clearly verify the assignment of methylene and methyl resonances. The pairs of methylene protons producing resonances 1 and 2, 3 and 4, 5 and 6, and 7 and 8 in Figure 6 are each part of separate ethyl groups.

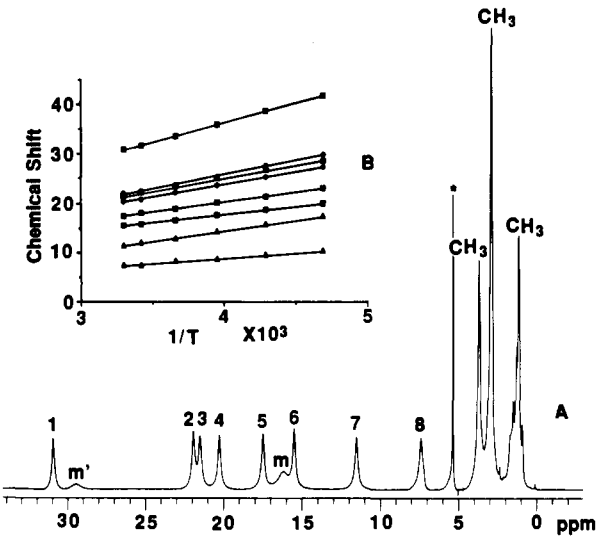

Figure 6. A, 300-MHz ^{1}H NMR spectrum of {(OEOP)Fe^{II}Cl} at 23 °C. Resonances are labeled in accord with those used in Figure 2 except that the resonances of the methylene protons are numbered 1–8. The peak denoted by an asterisk and the spikes around the upfield methyl resonances are impurities in the 100% dichloromethane-d_2. B, a plot of chemical shifts versus T^{-1} for the methylene resonances.

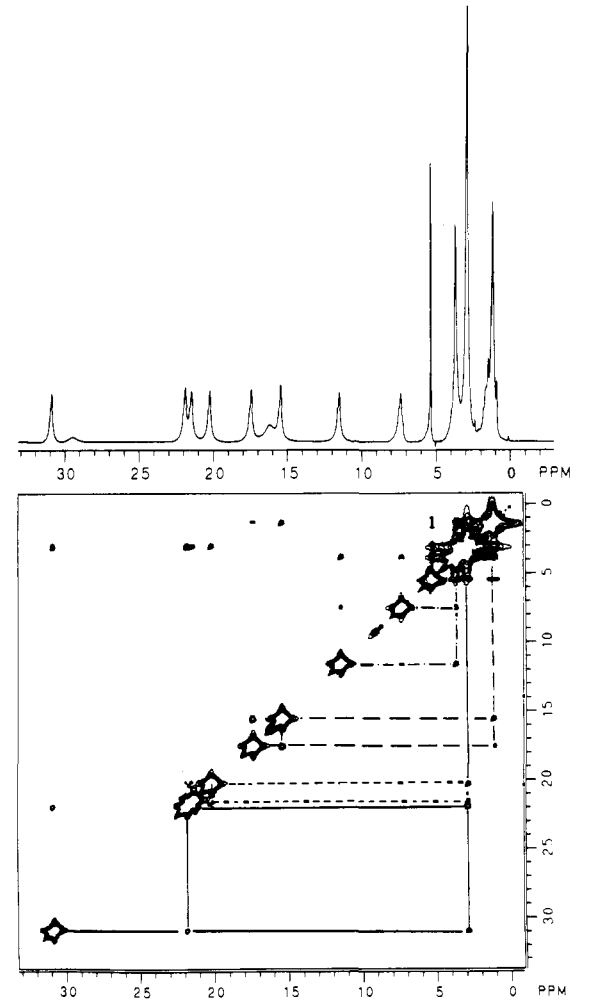

Figure 7. Top: 300-MHz ^{1}H NMR spectrum of {(OEOP)Fe^{II}Cl} in dichloromethane-d_2 at 30 °C. Bottom: 300-MHz ^{1}H MCOSY plot for this complex. Cross peaks between resonances of the four distinct ethyl groups are connected below the diagonal.

(23) Scheidt, W. R.; Reed, C. A. *Chem. Rev.* **1981**, *81*, 543.
(24) Scheidt, W. R.; Lee, Y. J. *Struct. Bonding* **1987**, *64*, 1.
(25) Skelton, B. W.; White, A. H. *Aust. J. Chem.* **1977**, *30*, 2655.

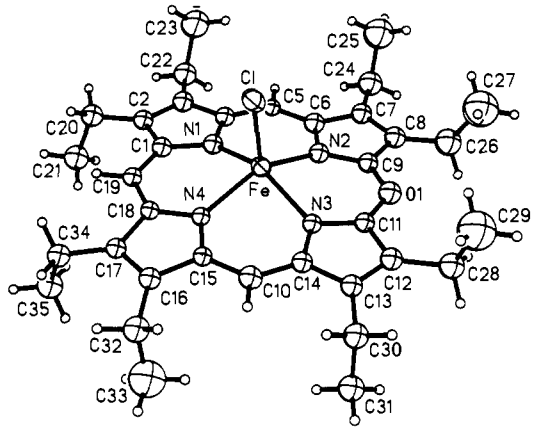

Figure 8. Perspective view of the structure of {(OEOP)Fe^{III}Cl} with 50% thermal contours for all atoms.

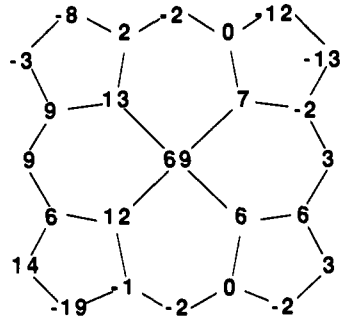

Figure 9. Diagram of the oxoporphyrin core for {(OEOP)Fe^{III}Cl}. Each atom symbol has been replaced by a number that represents the perpendicular displacement of that atom (in units of 0.01 Å) out of the mean oxoporphyrin plane.

The structure of {(OEOP)Fe^{III}Cl} has been studied by X-ray diffraction. A view of the complex, which has no crystallographically imposed symmetry, is shown in Figure 8. A selection of important bond distances and angles is given in Table II. The structure displays disorder in the location of the oxygen atom and one methine group. The structure has been refined to give 55% occupancy with O(1) and C(10), as shown in Figure 8, and 45% occupancy to a form with these two sites interchanged. Figure 8 only shows the major form. The other two methine groups are not affected by disorder.

The iron coordination conforms to expectations for high-spin, five-coordinate iron(II) in a porphyrin environment. The Fe–N distances average 2.094 Å, which is within the 2.072–2.096 Å range expected for similar porphyrin complexes of the high-spin, five-coordinate class.[23,24] The iron is displaced 0.69 Å out of the porphyrin plane. The Fe–Cl distance (2.307(3) Å) is slightly shorter than the Fe–Cl distance in high-spin {(N-MeTPP)Fe^{III}Cl} (2.329(2) Å).[25] The Fe–Cl is tilted slightly so that it makes an angle of 5.9° with respect to the N_4 plane. In order to accommodate the five-coordinate iron, the oxoporphyrin core is somewhat domed. This is best seen in Figure 9, which shows the displacements of each atom of the oxoporphyrin interior from the mean plane of this unit.

Electronic Structure of the Oxoporphyrin Macrocycle. Semiquantitative Fenske–Hall LCAO molecular orbital calculations[26] have been performed on the oxoporphyrin anion. These are approximate Hartree–Fock–Roothan SCF LCAtO molecular orbital calculations which depend only on the choice of wave function and use atomic coordinates as input data. The macrocycle structure was assumed to be fully planar, with typical C–C, C–N, and C–O distances chosen to achieve maximal symmetry.

In order to probe the charge distribution within the macrocycle, the Mulliken gross atomic charges for the oxoporphrin monoanion and the porphyrin dianion are compared in Table III. Important conclusions to be drawn from these data are as follow: the porphyrin core retains the dianionic nature in both porphyrin and oxoporphyrin, and the peripheral charge on the oxoporphyrin is increased. This increase, as shown by the values in the column Δ(O–C), is most pronounced in the vicinity of the oxo unit. The valley carbons (C(2)) have the greatest positive charge and are the sites most susceptible to nucleophilic attack, This is particularly significant, because the next step in porphyrin degradation is ring opening of the macrocycle to form biliverdin. This process appears to involve attack by hydroxide on the iron-coordinated oxoporphyrin at C(2).[3-5]

Figure 10 shows representations of the frontier π molecular orbitals for the oxoporphyrin anion along with their computed energies. These are of use in understanding the patterns of hyperfine shifts[27] in the NMR spectra of the iron oxoporphyrins.

Table II. Selected Interatomic Distances and Angles for {(OEOP)Fe^{III}Cl}

Bond Lengths (Å)			
Fe–Cl	2.307(3)	Fe–N(1)	2.091(6)
Fe–N(2)	2.104(6)	Fe–N(3)	2.100(6)
Fe–N(4)	2.082(6)	O(1A)–C(14)	1.382(9)
O(1A)–C(15)	1.392(8)	C(10)–C(14)	1.382(9)
C(10)–C(15)	1.392(8)	N(1)–C(1)	1.380(9)
N(1)–C(4)	1.351(10)	N(2)–C(6)	1.369(10)
N(2)–C(9)	1.352(8)	N(3)–C(11)	1.350(9)
N(3)–C(14)	1.372(10)	N(4)–C(15)	1.340(9)
N(4)–C(18)	1.362(8)	C(1)–C(2)	1.431(10)
C(1)–C(19)	1.409(11)	C(2)–C(3)	1.378(11)
C(5)–C(6)	1.369(9)	C(3)–C(4)	1.444(10)
C(7)–C(8)	1.330(10)	C(4)–C(5)	1.393(10)
C(8)–C(9)	1.463(11)	C(6)–C(7)	1.457(11)
C(9)–O(1)	1.364(9)	C(9)–C(10A)	1.364(9)
O(1)–C(11)	1.372(10)	C(10A)–C(11)	1.372(10)
C(11)–C(12)	1.434(10)	C(12)–C(13)	1.359(11)
C(16)–C(17)	1.361(10)	C(13)–C(14)	1.440(9)
C(17)–C(18)	1.458(11)	C(15)–C(16)	1.441(10)
C(18)–C(19)	1.378(10)		

Bond Angles (deg)			
Cl–Fe–N(1)	104.6(2)	Cl–Fe–N(2)	112.0(2)
N(1)–Fe–N(2)	85.9(2)	Cl–Fe–N(3)	108.6(2)
N(1)–Fe–N(3)	146.8(2)	N(2)–Fe–N(3)	83.0(2)
Cl–Fe–N(4)	101.1(2)	N(1)–Fe–N(4)	87.1(2)
N(2)–Fe–N(4)	146.9(2)	N(3)–Fe–N(4)	85.5(2)
C(14)–O(1A)–C(15)	126.4(6)	C(14)–C(10)–C(15)	126.4(6)
Fe–N(1)–C(1)	125.6(5)	Fe–N(1)–C(4)	126.7(4)
C(1)–N(1)–C(4)	106.3(6)	Fe–N(2)–C(6)	125.7(5)
Fe–N(2)–C(9)	127.4(5)	C(6)–N(2)–C(9)	105.3(6)
Fe–N(3)–C(11)	127.3(5)	Fe–N(3)–C(14)	125.7(5)
C(11)–N(3)–C(14)	103.7(5)	Fe–N(4)–C(15)	127.6(4)
Fe–N(4)–C(18)	125.6(5)	C(15)–N(4)–C(18)	105.8(6)
N(1)–C(1)–C(2)	110.5(6)	N(1)–C(1)–C(19)	122.8(6)
C(2)–C(1)–C(19)	126.6(6)	C(1)–C(2)–C(3)	106.2(6)
C(2)–C(3)–C(4)	106.5(7)	N(1)–C(4)–C(3)	110.6(6)
N(1)–C(4)–C(5)	124.4(6)	C(3)–C(4)–C(5)	125.0(7)
C(4)–C(5)–C(6)	127.3(7)	N(2)–C(6)–C(5)	124.5(7)
N(2)–C(6)–C(7)	110.2(6)	C(5)–C(6)–C(7)	125.2(7)
C(6)–C(7)–C(8)	107.3(7)	C(7)–C(8)–C(9)	105.8(6)
N(2)–C(9)–C(8)	111.4(6)	N(2)–C(9)–O(1)	124.8(7)
C(8)–C(9)–O(1)	123.8(6)	N(2)–C(9)–C(10A)	124.8(7)
C(8)–C(9)–C(10A)	123.8(6)	C(9)–O(1)–C(11)	126.2(6)
C(9)–C(10A)–C(11)	126.2(6)	N(3)–C(11)–O(1)	123.5(6)
N(3)–C(11)–C(10A)	123.5(6)	N(3)–C(11)–C(12)	112.8(7)
O(1)–C(11)–C(12)	123.7(6)	C(10A)–C(11)–C(12)	123.7(6)
C(11)–C(12)–C(13)	105.9(6)	C(12)–C(13)–C(14)	105.7(7)
O(1A)–C(14)–N(3)	124.1(6)	C(10)–C(14)–N(3)	124.1(6)
O(1A)–C(14)–C(13)	124.0(7)	C(10)–C(14)–C(13)	124.0(7)
N(3)–C(14)–C(13)	111.9(6)	O(1A)–C(15)–N(4)	124.7(6)
C(10)–C(15)–N(4)	124.7(6)	O(1A)–C(15)–C(16)	123.5(7)
C(10)–C(15)–C(16)	123.5(7)	N(4)–C(15)–C(16)	111.8(6)
C(15)–C(16)–C(17)	106.2(6)	C(16)–C(17)–C(18)	105.6(6)
N(4)–C(18)–C(17)	110.6(6)	N(4)–C(18)–C(19)	124.9(7)
C(17)–C(18)–C(19)	124.4(6)	C(1)–C(19)–C(18)	127.7(7)

(26) Hall, M. B.; Fenske, R. F. *Inorg. Chem.* **1972**, *11*, 768.

(27) La Mar, G. N.; Walker (Jensen) F. A. In *The Porphyrins*; Dolphin, D., Ed.; Academic Press: New York, 1979; Vol. 1VB, p 57.

Table III. Mulliken Gross Atomic Charges

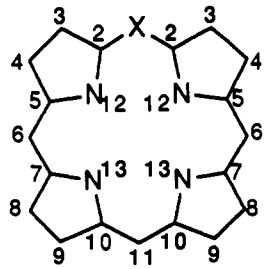

	porphyrin dianion (X = CH)	oxoporphyrin anion (X = O)	Δ(O–C)[a]
X	−0.304	−0.143	161
C(2)	0.331	0.535	204
C(3)	−0.172	−0.249	−77
C(4)	−0.172	−0.095	77
C(5)	0.332	0.332	0
C(6)	−0.308	−0.237	66
C(7)	0.331	0.328	−3
C(8)	−0.171	−0.147	24
C(9)	−0.173	−0.142	31
C(10)	0.333	0.323	−10
C(11)	−0.304	−0.224	80
N(12)	−0.537	−0.581	−40
N(13)	−0.537	−0.487	50
$\sum N^b$	−2.148	−2.136	20
P.C.[c]	0.148	1.136	

[a] Difference between the porphyrin and the oxoporphyrin charges. [b] Charge on the four nitrogen atoms. [c] Charge on the periphery of the macrocycle.

Orbitals Ψ_1 and Ψ_2 are empty and correspond to the well-known $4e_g^*$ orbitals of the porphyrin ring system. The orbitals designated Ψ_{-3} and Ψ_{-4} are filled and correspond to the a_{2u} and a_{1u} porphyrin orbitals. With regard to metal–ligand π bonding, these are nonbonding due to near 0 overlap. Orbitals Ψ_{-6} and Ψ_{-7} are also filled. They correspond to the porphyrin $3e_g$ orbitals.

Discussion

The results described above clearly establish that the iron(II) and iron(III) forms of the verdohemes contain the oxoporphyrin macrocycle **C**. Consequently, the verdohemochromes must have structure **A**, not structure **B**. The iron(III) complex **3** is six-coordinate and high-spin ($S = {}^5/_2$). The iron(II) complex **4** is also high-spin ($S = 2$) but five-coordinate.

The X-ray diffraction studies indicate that the oxoporphyrin ligand acts essentially like a porphyrin and that it coordinates as a planar tetradentate macrocycle. However, the core size is somewhat smaller than that of a corresponding porphyrin. This is seen by comparing the N_{Cl}–N distances in **3** and **4** with those of comparable porphyrin complexes. This contraction is fully expected since the covalent radius of oxygen is smaller than that of carbon. Unfortunately, due to the crystallographic disorder found in the structures of **3** and **4**, it is not possible to make a detailed comparison of the geometry at the oxo and methine bridges.

Despite the fact that the oxoporphyrin is geometrically similar to a porphyrin, it differs in its net charge, since it is a monoanion in its deprotonated form. As a consequence of its lower charge, it forms neutral complexes that differ from the corresponding porphyrin complexes. Thus, porphyrins form five-coordinate, high-spin iron(III) halo complexes ($PFe^{III}Cl$), whereas the oxoporphyrin forms six-coordinate, high-spin complexes. In this regard the oxoporphyrin resembles other porphyrins which have peripheral substituents that bear a positive charge. The crystal structure of six-coordinate {β-Ph_3P^+-TPP)$FeCl_2$} has recently been reported.[28] Related ^1H NMR studies have shown that iron(III) coordinates two axial bromide ions to form {β-py^+-TPP)$FeBr_2$}.[29]

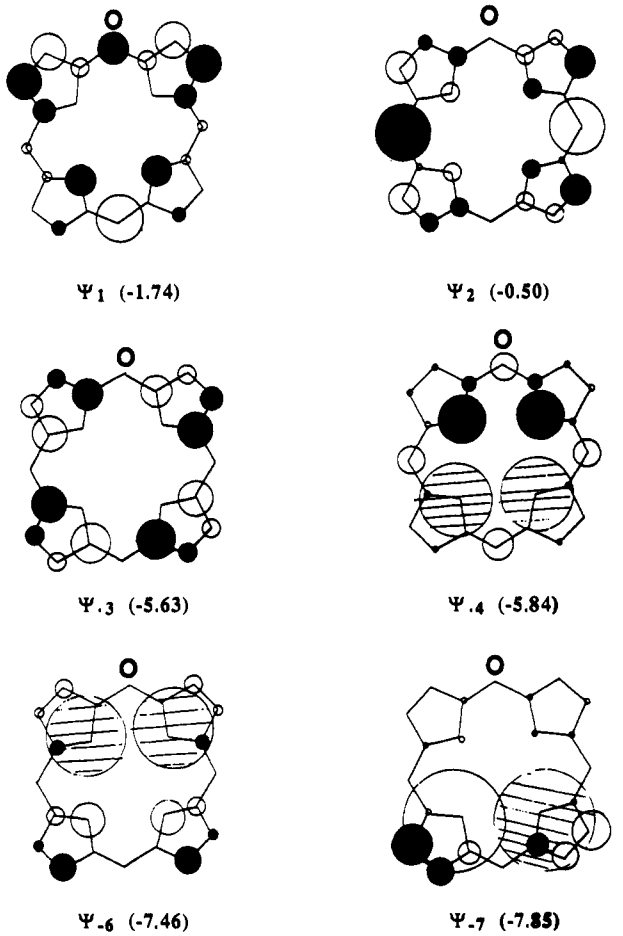

Figure 10. Representations of the π molecular orbitals for the oxoporphyrin dianion. Energies (eV) for each are shown in parentheses.

Iron(II) porphyrins have low affinity for axial coordination of halide ions, whereas the neutral five-coordinate oxoporphyrin complexes {(OEOP)Fe^{II}X} (X = Cl, Br) are readily isolated. It is important to note that it is probably overall charge, rather than core charge, which is responsible for the ready formation of these five-coordinate iron(II) complexes. N-Alkylated porphyrins and thiaporphyrins deprotonate to form monoanions with that charge residing in the core. These also form high-spin, five-coordinate halo complexes {N-MeTPP)$Fe^{II}Cl$}[30] and {(STPP)$Fe^{II}Cl$}.[31]

The structures of both [(OEOP)$Fe^{III}Br_2$] and {(OEOP)$Fe^{II}Cl$} suffer from disorder that involves the positioning of the oxo bridge. This disorder is in no way unexpected. Core modification of porphyrins results in an alteration of the interior portion of the macrocycle. Such a modification produces a negligible change in the external shape of the macrocycle. Since it is the external shape of the molecule that is largely responsible for the way it is oriented within a crystal, core modification is likely to result in structural disorder. Similar disorder has been seen for related core modified porphyrins: octaethylporphyrin *N*-oxide[32] and its nickel(II) complex,[33] thiaporphyrins,[34,35] and complexes of octaethyloxophlorin (meso-hydroxyoctaethylporphyrin).[36]

(28) Małek, A.; Latos-Grażyński, L.; Bartczak, T. J.; Żadło, A. *Inorg. Chem.* **1991**, *30*, 3222.

(29) Rachlewicz, K.; Latos-Grażyński, L., manuscript in preparation.

(30) Anderson, O. A.; Kopelove, A. B.; Lavallee, D. K. *Inorg. Chem.* **1980**, *19*, 2101.

(31) Latos-Grażyński, L.; Lisowski, J.; Olmstead, M. M.; Balch, A. L. *Inorg. Chem.* **1989**, *28*, 1183.

(32) Balch, A. L.; Chan, Y. W.; Olmstead, M. M.; Renner, M. W. *J. Am. Chem. Soc.* **1985**, *107*, 2393.

(33) Balch, A. L.; Chan, Y. W.; Olmstead, M. M. *J. Am. Chem. Soc.* **1985**, *107*, 6510.

(34) Latos-Grażyński, L.; Lisowski, J.; Olmstead, M. M.; Balch, A. L. *J. Am. Chem. Soc.* **1987**, *109*, 4428.

(35) Latos-Grażyński, L.; Lisowski, J.; Szterenberg, L.; Olmstead, M. M.; Balch, A. L. *J. Org. Chem.* **1991**, *56*, 4043.

The ^{1}H NMR spectra and the magnetic moment measurements indicate that {(OEOP)Fe^{III}X$_2$} has an $S = {}^5/_2$ ground state and that {(OEOP)Fe^{II}Cl} has an $S = 2$ ground state. In both cases the magnetic properties are also consistent with the structural data available from the X-ray crystallographic studies. Thus, the structural parameters for both complexes closely conform to what has been observed for high-spin, six-coordinate iron(III) and high-spin, five-coordinate iron(II) porphyrin complexes.[23,24]

The ^{1}H NMR spectral pattern seen for {(OEOP)Fe^{III}X$_2$} is related to the analogous spectra of high-spin, six-coordinate iron(III) porphyrin compounds. The latter have the methylene and meso protons shifted to low field. This general downfield bias can be attributed to a strong σ (nitrogen lone pair) contribution in the Fe–N bonds, which affects both the meso and pyrrole positions. The observation of a wide spread in methylene resonances in Figure 3 can be attributed to both inherent asymmetry in the σ framework and to L → M charge transfer in which the occupied orbitals Ψ_{-7} and Ψ_{-6} are involved. This latter mechanism would have a major effect on the spread of the methylene resonances but would not serve to differentiate the meso positions since these orbitals have essentially no contribution from the meso carbons. M → L charge transfer would involve the two vacant π orbitals Ψ_1 and Ψ_2. This would place a large amount of spin density at the meso positions. As in the case of six-coordinate iron(III) porphyrins, this contribution is probably negligible.

With iron(III) porphyrins, the chemical shift of the meso protons has been demonstrated to be a useful diagnostic probe for differentiating between five- and six-coordinate species.[37-39] Five-coordinate complexes have their meso proton resonances with an upfield chemical shift, while six-coordinate complexes display downfield shifts for these protons. The available ^{1}H NMR data for {(OEOP)Fe^{III}X$_2$} suggest that its electronic structure is similar to that of six-coordinate, high-spin iron(III) porphyrins.

The ^{1}H NMR spectra of {(OEOP)Fe^{II}X} differ from those of the iron(III) complexes, particularly in their greater complexity, which results from their lower symmetry. This produces eight methylene resonances for the five-coordinate iron(II) complexes, while four are observed for the six-coordinate iron(III) compounds.

As a result of this work, the physical and electronic structures of the paramagnetic iron(II) and iron(III) forms of the verdohemes are now clearly established.

Experimental Section

Preparation of Compounds. [(OEOP)Fe^{II}(py)$_2$]Cl. This was obtained by a variation on standard routes of verdohemochrome formation.[12,13] A 500-mg sample of ascorbic acid was added to a solution of 100 mg of (OEP)Fe^{II}(py)$_2$ in 6 mL of pyridine. A 50-mL portion of dichloromethane which was saturated with dioxygen was added. The mixture was shaken for 5 min. The green solution was filtered to remove any insoluble material, and the filtrate was washed with two 50-mL portions of water. The resulting green solution was dried by passage through a 5-cm-thick layer of anhydrous sodium sulfate. The sample was evaporated to dryness under vacuum to give a green, air-sensitive residue which was handled in a dioxygen-free environment. The solid was dissolved in 20 mL of dioxygen-free dichloromethane. A sample of 30 mL of dioxygen-free *n*-hexane was added. The volume of the sample was reduced under vacuum until a green precipitate formed. At this stage an additional 10-mL portion of *n*-hexane was added. The deep green precipitate was collected by filtration and washed with *n*-hexane to remove a dark blue-green substance (yield 52 mg, 50%). The isolated solid has spectroscopic features consistent with previous preparations of verdohemochrome. UV/vis absorption: (in pyridine) λ_{max} 384 (6.5×10^4), 494 (9.2×10^3), 526 (1.7×10^4), 651 (5.5×10^4). ^{1}H NMR: δ meso-H, 9.6(2), 9.1(1); methylene, 3.63(4) q, 3.51(4) q, 3.42, 3.40(8) overlapping q; methyl, 1.67(6) t, 1.63, 1.61(12) overlapping t, 1.55(6) t.

{(OEOP)Fe^{III}Cl$_2$}. [(OEOP)Fe^{II}(py)$_2$]Cl (20 mg) was dissolved in 20 mL of a saturated 2% solution of 12 M hydrochloric acid in methanol. The sample was filtered, and the solvent was removed under vacuum. The resulting green solid was recrystallized by dissolving it in a minimum volume of dichloromethane and slowly adding diethyl ether to precipitate the product as deep green crystals (yield 14 mg, 80%). UV/vis absorption: (in dichloromethane) λ_{max}, nm (ϵ, cm^{-1} M^{-1}), 372 (6.1×10^4), 468 sh (1.1×10^4), 536 (6×10^3), 627 (1.8×10^4), 82 (1.0×10^4), 712 (1.5×10^4). The ^{1}H NMR spectrum is shown in Figure 2.

{(OEOP)Fe^{III}Br$_2$}. This was prepared by the procedure used for {(OEOP)Fe^{III}Cl$_2$} except that hydrogen bromide replaced hydrogen chloride. UV/vis absorption spectrum: λ_{max}, nm, 364, 475, 582, 650, 720. ^{1}H NMR (dichloromethane-d_2, 23 °C) ppm (intensity) meso-H 39(1), 31(2); methylene-H, 48.5(4), 35.0(4), 34.0(4), 24.5(4); methyl-H broad resonance 5.8–5.0. Crystals of the complex suitable for X-ray crystallography were prepared by the slow diffusion of diethyl ether into a dichloromethane solution of the complex.

{(OEOP)Fe^{II}Cl}. Under an atmosphere of purified dinitrogen, 0.50 g of solid sodium dithionite was added to a solution of 10 mg (0.015 mmol) of {(OEOP)Fe^{III}Cl$_2$} in 10 mL of dioxygen-free dichloromethane. The green mixture was stirred for 2 h. The solution was filtered to remove the excess sodium dithionite, and the filtrate was evaporated to dryness. The product may be recrystallized from dichloromethane/diethyl ether (yield 9.4 mg, 100%). UV/vis absorption: (in dichloromethane) λ_{max}, nm (ϵ, cm^{-1} M^{-1}), 328 (4.3×10^4), 394 (5.9×10^4), 518 (9.5×10^3), 550 (9.7×10^3), 662 (6.3×10^4). The ^{1}H NMR spectrum is shown in Figure 5. Crystals suitable for X-ray diffraction were grown by diffusion of diethyl ether into a dichloromethane solution of the complex.

X-ray Data Collection. {(OEOP)Fe^{III}Br$_2$}. A suitable crystal was coated with a light hydrocarbon oil and mounted in the 130 K dinitrogen stream of a Syntex P2$_1$ diffractometer equipped with a locally modified LT-1 low-temperature apparatus. Crystal data are given in Table IV. Two check reflections showed only random (<2%) variation in intensity during data collection. The data were corrected for Lorentz and polarization effects.

{(OEOP)Fe^{III}Cl}. A dark green needle was coated with a light hydrocarbon oil and mounted in the 130 K dinitrogen stream of a Siemens P4/RA diffractometer equipped with a LT-2 low-temperature device. Only random fluctuations (<2%) in the intensities of two standard reflections were observed during data collection. Crystal data are presented in Table IV. Corrections for Lorentz and polarization effects were applied.

Solution and Structure Refinement. Calculations were performed on a DEC VAX station 3200 with SHELXTL Plus version 4.00. Scattering factors and corrections for anomalous dispersion were taken from a standard source.[40] Absorption corrections were applied to each structure.[41] The solution for each compound was determined from the

Table IV. Crystal Data and Data Collection Parameters

	3	4
formula	$C_{39}H_{53}Br_2FeN_4O_2$	$C_{35}H_{43}ClFeN_4O$
fw	837.6	627.0
color and habit	dark red block	dark green needle
crystal system	monoclinic	monoclinic
space group	$C2/m$	$P2_1/c$
a, Å	13.521(5)	12.706
b, Å	17.516(8)	13.408(2)
c, Å	8.289(3)	19.498(4)
β, deg	107.75(2)	103.69(2)
V, Å^3	1869.7(13)	3227.3(11)
T, K	130	130
Z	2	4
cryst dimens, mm	0.20 × 0.32 × 0.36	0.13 × 0.13 × 0.38
d_{calcd}, g cm^{-3}	1.488	1.290
radiation (λÅ)	Mo Kα (0.710 69)	Cu Kα (1.541 84)
μ, mm^{-1}	2.723	4.761
range of transmission factors	0.31–0.64	0.56–0.60
no. of data collected	3582	2845
no. of unique data	1713	2469
no. of data used in refinement	1503 ($I > 3\sigma(I)$)	2171 ($I > 2\sigma(I)$)
no. of parameters refined	105	180
R^a	0.061	0.069
$R_w{}^a$	0.051	0.108

$^a R = \sum||F_o| - |F_c||/|F_o|$ and $R_w = \sum||F_o| - |F_c||w^{1/2}/\sum|F_o|w^{1/2}$.

(36) Balch, A. L.; Noll, B. C.; Zovinka, E. P. *Inorg. Chem.* **1992**, *31*, 2248.
(37) Budd, D. L.; La Mar, G. N.; Langry, K. C.; Smith, K. M.; Mayyir-Mazhir, R. *J. Am. Chem. Soc.* **1979**, *101*, 6091.
(38) Morishima, I.; Shiro, Y.; Wakino, T. *J. Am. Chem. Soc.* **1985**, *107*, 1063.
(39) Rajarathnam, K.; La Mar, G. N.; Chiu, M. L.; Sligar, S. G.; Singh, J. P.; Smith, K. M. *J. Am. Chem. Soc.* **1991**, *113*, 7886.
(40) *International Tables for X-ray Crystallography*; Kynoch Press: Birmingham, England, 1974; Vol. 4.
(41) The method obtains an empirical absorption tensor from an expression relating F_o and F_c. Moezzi, B. Ph.D. Thesis, University of California, Davis, 1987.

Patterson maps and subsequent cycles of least-squares refinement and calculation of difference Fourier maps.

{(OEOP)$Fe^{III}Br_2$}. There is disorder in the oxygen atom location, and carbon atom C(1) was refined as coincident with O(1). Hydrogen atoms were located on a difference map and fixed at ideal geometries for subsequent cycles of least-squares refinement. A difference map showed a peak with intensity of 0.5 e/Å^3 that was 1.1 Å from C(1). This was added to the model of the structure at fixed, ideal geometry, and four more cycles of full-matrix least-squares refinement were run. The unit cell contains two molecules of diethyl ether which are disordered across a mirror plane and a 2-fold axis. After many different models were tried, a group of five atoms was selected that best approximate the diethyl ether. The positional parameters for this molecule were ultimately fixed, the occupancies were set at 0.25, and only isotropic thermal parameters were refined. During final stages of refinement, all the remaining nonhydrogen atoms were assigned anisotropic thermal parameters. The largest peak in the final difference map is 2.26 Å from Br and has an electron density of 1.2 e/Å^3.

{(OEOP)$Fe^{II}Cl$}. There is disorder in the occupancy at the sites of O(1) and C(10). The arrangement shown in Figure 8 has a computed occupancy of 55(3)%. The other arrangement interchanges O(1) and C(10).

Instrumentation. ^{1}H NMR spectra were recorded on a General Electric QE-300 FT NMR spectrometer operating in the quadrature mode (^{1}H frequency is 300 MHz). The spectra were collected over a 50-kHz bandwidth with 16K data points and a 5-μs 45° pulse. For a typical spectrum, between 1000 and 5000 transients were accumulated with a 50-ms delay time. The signal-to-noise ratio was improved by apodization of the free inducting decay. Electronic spectra were obtained using a Hewlett-Packard diode array spectrometer.

The MCOSY spectra were obtained as described previously[22] after a standard 1D reference spectrum was collected. The 2D spectra were collected by the use of 1024 points in t_2 that were collected over the bandwidth necessary to include the desired resonances with 512 t_1 blocks and 1024 scans per block. These were zero filled to 1024 t_2 × 1024 t_1. All experiments included four dummy scans prior to collection of the first block.

Acknowledgment. We thank the NIH (GM-26226) for financial support.

Supplementary Material Available: Tables of atomic positional parameters, bond distances, bond angles, anisotropic thermal parameters, and crystal data for {(OEOP)$Fe^{III}Br_2$} and {(OEOP)$Fe^{II}Cl$} (17 pages); observed and calculated structure factors (16 pages). Ordering information is given on any current masthead page.

η^2-Coordination and C-F Activation of Hexafluorobenzene by Cyclopentadienylrhodium and -iridium Complexes

Simon T. Belt,[1a] Madeleine Helliwell,[1a] William D. Jones,[1b] Martin G. Partridge,[1a] and Robin N. Perutz*,[1a]

Contribution from the Departments of Chemistry, University of York, Heslington, York, YO1 5DD, U.K., and University of Rochester, Rochester, New York 14627.
Received August 17, 1992

Abstract: The photochemical reaction of (η^5-C_5R_5)$Rh(PMe_3)(C_2H_4)$ (R = H, Me) with hexafluorobenzene yields (η^5-C_5R_5)$Rh(PMe_3)(\eta^2$-$C_6F_6)$. The structure of (η^5-C_5H_5)$Rh(PMe_3)(\eta^2$-$C_6F_6)$ has been determined crystallographically (a = 10.533, b = 11.271, c = 13.074 Å, orthorhombic, space group *Pnma*, Z = 4). The C_6F_6 ligand is bound through two carbons and is distorted to generate a planar C_6F_4 unit with the two remaining C-F bonds at 43.8° to the plane. Several reactions of (η^5-C_5H_5)$Rh(PMe_3)(\eta^2$-$C_6F_6)$ are reported which yield (η^5-C_5H_5)$Rh(PMe_3)$L or (η^5-C_5H_5)$Rh(PMe_3)$(X)Y (L = CO, PPh_3; X = Ph, Si^iPr_3, Y = H; X = Y = Cl) either photochemically or thermally. The extended photolysis of (η^5-C_5Me_5)Rh-$(PMe_3)(\eta^2$-$C_6F_6)$ generates a second product assigned as (η^5-C_5Me_5)$Rh(PMe_3)(C_6F_5)$F. The chlorination of this complex yields (η^5-C_5Me_5)$Rh(PMe_3)(C_6F_5)$Cl. The crystal structure of the latter (a = 14.129 (4), b = 9.610 (7), c = 30.320 (5) Å, β = 94.88 (5)°, monoclinic, space group $C2/c$, Z = 8) reveals a sterically congested molecule with the C_6F_5 group lying in a plane at an angle of 20° to the plane of the C_5Me_5 ring. The isolation and subsequent photolysis of (η^5-C_5Me_5)$Rh(PMe_3)(\eta^2$-$C_6F_6)$ in C_6F_6 also generates the C-F activation products. The thermal reaction of (η^5-C_5Me_5)$Rh(PMe_3)(C_6H_5)$H in C_6F_6 yields only the η^2-C_6F_6 complex, (η^5-C_5Me_5)$Rh(PMe_3)(\eta^2$-$C_6F_6)$. The results indicate that C_6F_6 reacts with the (η^5-C_5Me_5)$Rh(PMe_3)$ fragment in two sequential steps, with the formation of (η^5-C_5Me_5)$Rh(PMe_3)(\eta^2$-$C_6F_6)$ required before C-F insertion occurs. The photolysis of (η^5-C_5H_5)$Ir(PMe_3)H_2$ in C_6F_6 generates (η^5-C_5H_5)$Ir(PMe_3)(\eta^2$-$C_6F_6)$ and (η^5-C_5H_5)$Ir(PMe_3)(C_6F_5)$H concurrently. ^{2}H labeling studies show that the hydride ligand of the product derives from the hydride of the precursor. This CF insertion reaction is postulated to proceed via a ring slip or hydrogen-transfer mechanism, independently of the formation of (η^5-C_5H_5)$Ir(PMe_3)(\eta^2$-$C_6F_6)$. Irradiation of (η^5-C_5R_5)$Rh(PMe_3)(\eta^2$-$C_6F_6)$ (R = H, Me) in Ar matrices at 12 K results in two competing photochemical reactions: the first yields C_6F_6 and $CpRh(PMe_3)$ and the second generates the C-F insertion product, (η^5-C_5R_5)$Rh(PMe_3)(C_6F_5)$F. The expelled C_6F_6 and the insertion products are identified by their characteristic IR spectra. Dissociation of C_6F_6 is far more important for the (η^5-C_5H_5) than for the (η^5-C_5Me_5) complex. When (η^5-C_5H_5)-$Rh(PMe_3)(\eta^2$-$C_6F_6)$ is photolyzed in N_2 matrices, the $CpRh(PMe_3)$ fragment is trapped to form (η^5-C_5H_5)$Rh(PMe_3)(N_2)$. In CO-doped argon matrices, trapping results in formation of (η^5-C_5H_5)$Rh(PMe_3)$CO, and formation of the insertion product is suppressed.

Introduction

Partial coordination of arenes to transition metals (i.e., η^2- or η^4-coordination) may be considered either as a step toward full (η^6) coordination (eqs 1 and 2) or as a step toward oxidative addition (eq 3). The coordination/decoordination process may be induced by removal/addition of other ligands (eq 1), by irradiation, or by electron transfer (eq 2).[2] If we are to arrest these reactions at the η^2- or η^4-arene stage, there are three parameters

(1) (a) University of York. Present address of S.T.B.: Department of Chemistry, University of Ottawa, Ottawa, Ontario, Canada K1N 6N5. Present address of M.H.: Department of Chemistry, University of Manchester, Manchester, M13 9PL, U.K. (b) University of Rochester.

(2) Pierce, D. T.; Geiger, W. E. *J. Am. Chem. Soc.* **1989**, *111*, 7636. Bowyer, W. J.; Geiger, W. E. *J. Electroanal. Chem.* **1988**, *239*, 253; *J. Am. Chem. Soc.* **1985**, *107*, 5657. Bowyer, W. J.; Merkert, J. W.; Geiger, W. E.; Rheingold, A. L. *Organometallics* **1989**, *8*, 191.

0002-7863/93/1515-1429$04.00/0 © 1993 American Chemical Society